Advances in Nano Research, *Vol. 14, No. 6 (2023) 507-519*
https://doi.org/10.12989/anr.2023.14.6.507

Antibacterial mesoporous Sr-doped hydroxyapatite nanorods synthesis for biomedical applications

Gopalu Karunakaran*[1], Eun-Bum Cho**[1], Keerthanaa Thirumurugan[2], Govindan Suresh Kumar[3], Evgeny Kolesnikov[4] and Selvakumar Boobalan[2]

[1]*Institute for Applied Chemistry, Department of Fine Chemistry, Seoul National University of Science and Technology (Seoul Tech), 232 Gongneung-ro, Nowon-gu, Seoul 01811, Republic of Korea*
[2]*Department of Biotechnology, K.S. Rangasamy College of Arts and Science (Autonomous), Tiruchengode 637 215, Tamil Nadu, India*
[3]*Department of Physics, K.S. Rangasamy College of Arts and Science (Autonomous), Tiruchengode 637 215, Tamil Nadu, India*
[4]*Department of Functional Nanosystems and High-Temperature Materials, National University of Science and Technology "MISiS," Leninskiy Pr. 4, Moscow 119049, Russia*

(*Received December 7, 2021, Revised March 13, 2023, Accepted April 10, 2023*)

Abstract. Postsurgical infections are caused by implant-related pathogenic microorganisms that lead to graft rejection. Hence, an intrinsically antibacterial material is required to produce a biocompatible biomaterial with osteogenic properties that could address this major issue. Hence, this current research aims to make strontium-doped hydroxyapatite nanorods (SrHANRs) via an ethylene diamine tetraacetic acid (EDTA)-enable microwave mediated method using *Anodontia alba* seashells for biomedical applications. This investigation also perceives that EDTA acts as a soft template to accomplish Sr-doping and mesoporous structures in pure hydroxyapatite nanorods (HANRs). The X-ray diffraction (XRD) and transmission electron microscopy (TEM) analysis reveals the crystalline and mesoporous structures, and Brunauer–Emmett–Teller (BET) indicates the surface area of all the samples, including pure HANRs and doped HANRs. In addition, the biocidal ability was tested using various implant-related infectious bacteria pathogens, and it was discovered that Sr-doped HANRs have excellent biocidal properties. Furthermore, toxicity evaluation using zebrafish reports the non-toxic nature of the produced HANRs. Incorporating Sr^{2+} ions into the HAp lattice would enhance biocompatibility, biocidal activity, and osteoconductive properties. As a result, the biocompatible HANRs materials synthesized with Sr-dopants may be effective in bone regeneration and antibacterial in-built implant applications.

Keywords: *Anodontia alba*; biocompatibility; antibacterial activity; biomedical applications; mesoporous hydroxyapatite nanorods; strontium; toxicity

1. Introduction

Research on biogenic calcium phosphate used in orthopedics and bone tissue implants has increased recently (Um *et al*. 2020). A further increase in this area of research to obtain a better biomaterial, especially calcium phosphate, in particular hydroxyapatite, is enormously extended (Nakayama *et al*. 2018). Hydroxyapatite (HAp) materials have good biocompatibility, in addition to osteoconductive ability and bone regeneration (Rabiei *et al*. 2020).

Hence, due to its versatility, it is used in diverse biomedical applications like nanocarriers (Suchanková *et al*. 2020), biomedical coating (Naseri *et al*. 2021), wound healing (Tao *et al*. 2021), scaffolds (Feng *et al*. 2022, Maleki-Ghaleh *et al*. 2021, Shuai *et al*. 2022, 2021), implant applications (Oner *et al*. 2021), tissue engineering (Bhat *et al*. 2021), and dermal filler applications (Hwang *et al*. 2021). The implant application is the most commonly used for fast recovery applications among the aforementioned applications. However, during the usage of HAp as an implant material, there is a drawback of bacterial infection post-implantation (Garg *et al*. 2021). Thus, assimilation of intrinsic antibacterial HAp material is currently required research. Several researchers developed different nanoparticles, such as gold-silver (Au-Ag) bimetallic nano-mushrooms (Fu *et al*. 2021), strontium oxide (Apsana *et al*. 2018), silver nanoparticles (Balaz *et al*. 2019, Supraja *et al*. 2018), iron oxide (Madubuonu *et al*. 2020), and zinc oxide (Koutu *et al*. 2019), as excellent antibacterial materials for various biomedical applications. Fu *et al*. 2021, confirmed that the Au-Ag bimetallic nano-mushrooms were highly biocompatible and showed excellent inhibition capability against *Escherichia coli*. These nanoparticles have broad antibacterial activity. Apsana *et al*. 2018, synthesized strontium oxide (SrO) nanoparticles using *Ocimum sanctum* L. leaf extracts, which were found to be 42 nm in size and have excellent antibacterial properties towards *Staphylococcus aureus, Escherichia coli, Proteus vulgaris, Pseudomonas aeruginosa, Morganella morganii, and Klebsiella pneumoniae*. Based on the findings of the prior studies, we chose strontium (Sr) as a doping material to induce antibacterial properties in HAp for various biomedical applications.

Furthermore, the incorporation of various metal ions, such as terbium (Paduraru *et al*. 2021), europium (Liu *et al*.

*Corresponding author, Ph.D.,
E-mail: karunakarang5@seoultech.ac.kr
**Corresponding author, Professor
E-mail: echo@seoultech.ac.kr

ISSN: 2287-237X (Print), 2287-2388 (Online)

2021), silver (Bolli *et al*. 2021), cobalt (Bhattacharjee *et al*. 2020), and iron (Balakrishnan *et al*. 2021), in HAp improves the overall performance of the biomaterials in the living system. The substitution of HAp ensures bio-compatibility and osteoconductive ability in accordance with the provisions in the use of bone replacements (Arcos and Vallet-Regí 2020). Recent advances in nanomedicine have assisted in developing the aforementioned bone tissue engineering approaches for insufficient mechanical properties and ineffectual cell growth, which can facilitate the osteogenic regeneration of cells at defective sites (Wei and Dai 2021). The revival of interest in this arena has led to new expansions in terms of new doped calcium phosphate materials for use in orthopedics.

Among the naturally occurring elements present in living systems (Niehoff *et al*. 2020, Wood 2004), strontium is an essential element that has a diverse role throughout the human body (Pors Nielsen 2004). The first awareness of strontium came to light when a drug named strontium ranelate was introduced and was used to reduce the risk of fractures in patients who have osteoporosis (Pilmane *et al*. 2017). According to the nutritional data, an average man takes 1.9 mg of Sr per day in the form of food and fluids, of which we lose 0.34 mg in urine and 1.5 mg in stool, as well as other forms like sweat and hair (Szabo 2017). In addition, Sr is used in medicine and biochemical kinetic studies (Pors Nielsen 2004). However, Sr behaves exactly like Ca in the human body. A slight variation is observed with Sr because of its larger ionic size. Sr was also found to have common transport and absorption mechanisms in different human body organs (Pors Nielsen 2004). There have been no reports of toxic symptoms caused by Sr in the human body up to this point. Hence, due to its biological importance, we have aimed to incorporate Sr into the HAp during synthesis.

Globally, years of anticipated statistical transformation in residents have increased the utilization of auxiliary therapies, providing beneficial, long-term economic rejuvenation solutions. With the application of HAp in different fields, the demand for the synthesis of HAp is increasing daily. It is possible to synthesize HAp using various methods, including mechanical milling (Nordin *et al*. 2015), chemical precipitation (Mondal *et al*. 2016), hydrothermal mediation (Sun *et al*. 2018), and microwave method (Cai *et al*. 2019). However, the microwave-mediated hydrothermal method is less available but is an excellent method for high-purity HAp synthesis. The microwave-mediated method is a rapid process, and it leads to the synthesis of highly crystalline structures (Cai *et al*. 2019). Several attempts have been made to synthesize HAp from biosources such as eggshells (George *et al*. 2020), cuttlefish (Balu *et al*. 2020), natural gypsum (El-Maghraby and Greish, 2021), seashells (Ayyanar *et al*. 2020), bones (Abifarin *et al*. 2019), and corals (Siswanto *et al*. 2020), which is also an eco-friendly method. However, the synthesis of Sr-doped HAp using *Anodontia alba* seashells was not available till today. *Anodontia alba* is a very common edible clam that is also a bivalve mollusc that belongs to the family *Lucinidae* (Moore and Lopez 1970). Every year, several million tons of seashell waste are dumped into the environment, which leads to environmental pollution. As a result, converting this waste into useful HAp would be a better waste-to-wealth approach. Therefore, in this study, we utilized *Anodontia alba* seashells as a calcium source to convert into useful HAp.

Further, a mesoporous structure is essential to enhance the surface contact of the material for fast recovery and effective antibacterial material (Molino *et al*. 2020). Furthermore, it was recently demonstrated that mesoporous structure improved bone recovery (Molino *et al*. 2020). We utilized ethylene diamine tetraacetic acid (EDTA) as a chelating and surface-modifying agent to obtain a mesoporous structure. Several attempts are already available that prove that EDTA is used as a catalytic agent, precipitating agent, modifier, and chelating agent for the synthesis of several nanoparticles for different applications (Jang *et al*. 2018, Javed *et al*. 2020, Ranjeh *et al*. 2020, Yi *et al*. 2014). However, no report on the synthesis of Sr-doped mesoporous HAp *via* a microwave hydrothermal approach has been published.

The present study aimed to use *Anodontia alba* seashells to synthesize HAp, employing eco-friendly microwave hydrothermal synthesis. This method would be an eco-friendly approach in which the bio-waste would be converted into useful HAp biomaterials. The influence of the EDTA chelating agent will also be evaluated. The impact of Sr doping on HAp will also be assessed using different characterization techniques. Furthermore, the effect of Sr-doped HAp on zebrafish will also be evaluated for confirmation of biocompatibility. In addition, the antibacterial properties of Sr-doped HAp will also be assessed to check and validate its biocidal activity.

2. Experimental methods

2.1 Materials and synthesis of Sr-doped HAp using bio-waste seashells

EDTA was used as a chelating agent and a modifying agent during the synthesis. *Anodontia alba* seashells were used as calcium sources, and potassium phosphate was used as a phosphate source during the synthesis of HAp. The synthesis was performed by taking 11.2 g of *Anodontia alba* seashell powder and mixing it with 33.4 ml of HCl, allowing it to completely solubilize the seashell powder. After that, the above mixture was made up to 100 ml using distilled water. This solution acts as a calcium precursor solution. To this solution, 100 ml of potassium phosphate (0.6 M) was added dropwise under continuous stirring at 37 °C. Once the calcium precursor and phosphate precursor were mixed with the help of potassium hydroxide, the pH was adjusted to 13. Once pH 13 was achieved, the solution was kept under microwave hydrothermal treatment for 1 h at 900 W. After the microwave hydrothermal reaction, the obtained mixture was collected and washed several times to remove the non-reactants. When the washing is finished, the final precipitate is dried at 90 °C for 24 to 48 hours. After the powder was dried, it was crushed into fine powders and denoted as pure hydroxyapatite nanorods (HANRs).

skMeanwhile, Sr-doped samples were prepared by using strontium chloride ($SrCl_2$) at different mol.% ratios of 1, 3, and 5. The resultant samples were so-called SrHANRs-1, SrHANRs-2, and SrHANRs-3, respectively.

2.2 Characterization

The *Anodontia alba* seashells were characterized by Scanning Electron Microscopy - Energy Dispersive X-Ray Analysis (SEM-EDX) using Tescan Vega 30 to identify the elemental composition and its structures. The synthesized resultant samples of pure HANRs, SrHANRs-1, SrHANRs-2, and SrHANRs-3 are analyzed *via* diverse techniques. The X-ray diffraction method is used to identify the crystal lattice, size, and lattice parameters using an X-ray diffractometer (Difray-401, JSC, Russia), with Cr (chromium) as the primary X-ray source (λ = 2.2909 Å). The obtained spectrum was matched with typical standard ICCD - XRD configurations. Furthermore, unit cell parameters (*a*, *c*, and *V*) were measured using the standard formula (Jenkins and Snyder 1996). A Nicolet 380 Fourier transform infrared (FT-IR) spectrometer, Thermo DXR Raman Microscope, and energy-dispersive X-ray analyzer (EDX) (SSD-Japan) were used to obtain FT-IR, Raman, and EDX spectra to identify the functional groups, elements, and chemical composition present in it. Adsorption-desorption isotherms using nitrogen gas were examined with the help of the Nova 1200e analyzer (Quantachrome Instruments, USA) to analyze the surface area, pore size, and pore volume. The zeta potentials and morphological features of the created pure HANRs and Sr-doped HANRs samples were additionally measured through the Zetasizer (Malvern, UK) and transmission electron microscopy (TEM).

2.3 Antibacterial assay

To assess the antimicrobial potential of the samples, the synthesized samples were treated against two diverse bacterial strains, like *Klebsiella pneumoniae* and *Staphylococcus aureus*. The standard procedure disc diffusion method using nutrient agar (media) was performed (Ahmed *et al*. 2013). The freshly prepared cultures of the above strains were incubated at room temperature for 24 h. Moreover, solidified nutrient medium upon the Petri plates were placed with the pre-inoculated disk made from 0.12 g of powder (together with pure HANRs, SrHANRs-1, SrHANRs-2, and SrHANRs-3) and then incubated at 37 °C for 24 h. Consequently, the results were observed and recorded after an incubation period based on the width of zone inhibition (mm).

2.4 Evaluation of toxicity using the zebrafish model

The obtained samples (pure HANRs, SrHANRs-1, SrHANRs-2, and SrHANRs-3) were subjected to toxicity studies with zebrafish embryos, according to OECD-23 guidelines (Sudha *et al*. 2020). About 30 zebrafish embryos were selectively grouped as marked and unmarked. The marked embryos were dispersed at various proportions and detached using Hank's solution of 100 ml with several ratios (25-250 µg/ml) of attained pure HANRs, SrHANRs-1, SrHANRs-2, and SrHANRs-3. Later, the above solution was dispensed into different ampoules, and the development of organs was observed by light field microscopy. Furthermore, the dead and viable cells were checked and monitored in triplicate. A statistical study was conducted to prompt triplicates, and the analysis was performed using IBM (International Business Machines) SPSS (Statistical Package for Social Sciences) statistical software. After carrying out all the extensive studies, analysis of variance (ANOVA) was performed for all the results to test for a significant difference between groups, and the data were represented as mean ± SD.

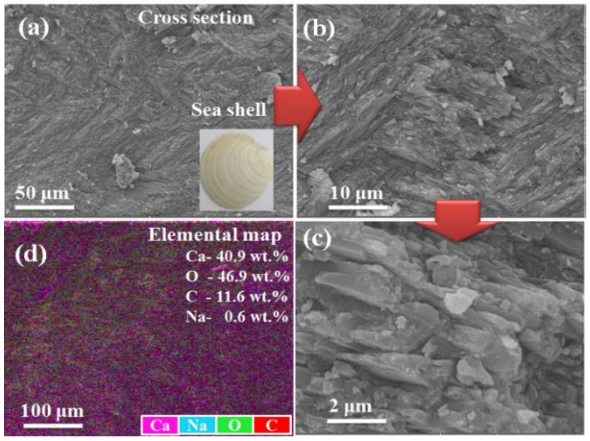

Fig. 1 (inset) *Anodontia alba*sea shell, (a, b, c) SEM image of the cross-section of sea shell under different magnifications, and (d) EDX elemental mapping of the seashell

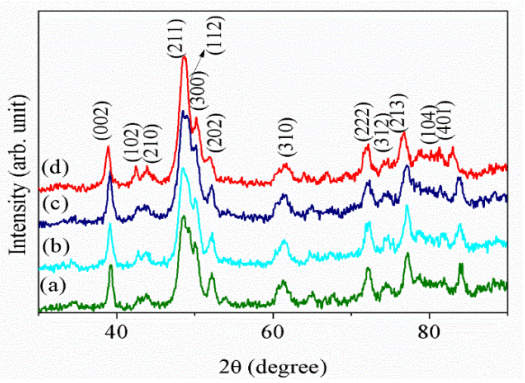

Fig. 2 XRD patterns of (a) pure HANRs, (b) SrHANRs-1, (c) SrHANRs-2 and (d) SrHANRs-3

3. Results and discussion

Fig. 1(a) inset corresponds to the picture of the *Anodontia alba* seashell used in this study. Meanwhile, morphological analysis of the seashell reveals the magnified images describing thin layers of 3–5 µm diameter crystals of poly aragonite attached to the organic matrix (Fig. 1(a)-(c)). Elemental analysis reports indicating the presence of calcium (Ca), sodium (Na), carbon (C), and oxygen (O) in a seashell were represented in EDX spectral analysis (Fig. 1(d)).

Table 1 Lattice parameters of HAp crystalline phase present in the synthesized samples

Sample code	Lattice constants (Å)		Unit cell volume, V ($Å^3$)	Lattice distortion (c/a)
	$a = b$	c		
Pure HANRs	9.3824	6.8450	521.84	0.7295
SrHANRs-1	9.3693	6.8662	521.99	0.7328
SrHANRs-2	9.3673	6.8612	522.15	0.7335
SrHANRs-3	9.3607	6.8558	522.47	0.7339

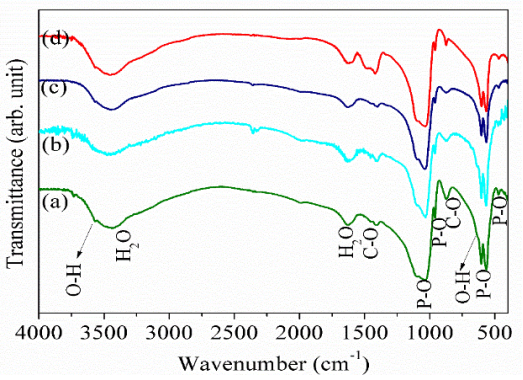

Fig. 3 FTIR spectra of (a) pure HANRs, (b) SrHANRs-1, (c) SrHANRs-2 and (d) SrHANRs-3

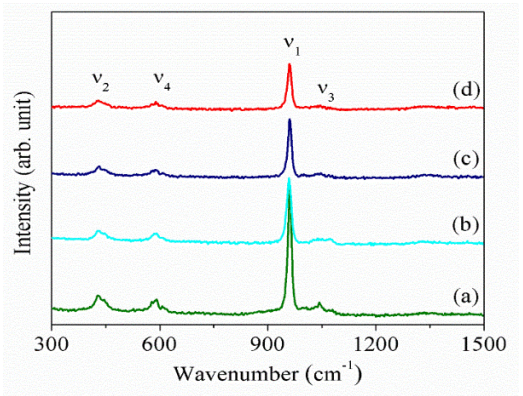

Fig. 4 Raman spectra of (a) pure HANRs, (b) SrHANRs-1, (c) SrHANRs-2 and (d) SrHANRs-3

To determine the crystal structures of the synthesized samples, X-ray diffraction was carried out determining the 2θ values corresponding to Miller's planes for pure HANRs samples indexed as 39.15° (002), 42.27° (102), 44.46° (210), 48.13° (211), 49.12° (112), 49.89° (300), 51.56° (202), 60.68° (310), 64.17° (311), 72.24° (222), 74.43° (312), 77.12° (213), 80.11° (321), 81.32° (104), and 83.42° (401) (Fig. 2). The XRD patterns were in agreement with the standard JCPDS (09-0432) data of the HAp, which indicate that the manufactured HAp are hexagonal crystallographic HAp (Kumar *et al*. 2018a).

In addition, the 2θ values confirming to Miller's planes for SrHANRs-1 samples were indexed as 39.17° (002), 42.29° (102), 44.36° (210), 48.17° (211), 49.23° (112), 49.78° (300), 51.37° (202), 60.76° (310), 64.21° (311), 72.32° (222), 74.23° (312), 77.15° (213), 80.15° (321), 81.23° (104), and 83.52° (401) (Fig. 2). SrHANRs-2, and SrHANRs-3 also display similar peak values to those of the SrHANRs-1 samples. The strontium (Sr) is readily incorporated into the HAp lattice instead of Ca ions, as both the size ratio and ionic radius are similar (Liu *et al*. 2020). The substitution of strontium (Sr) in the HAp crystal is significant as it plays a leading role in bone metabolism and treating osteoporotic disorders. Further, it was interesting to note that the substitution of strontium in the β-TCP lattice structure was achieved without affecting the HAp crystal lattice.

The results of this study agree well with the study reported (Zhou *et al*. 2021), in which the incorporation of strontium ions did not change the functional group but altered crystallinity due to the dopant concentration. Another study demonstrated that incorporating strontium ions can stabilize the apatite phase (Yuan *et al*. 2021). Besides, XRD peaks are most likely attributed to variances in diffraction peak intensities associated with pure HANRs, SrHANRs-1, SrHANRs-2, and SrHANRs-3 samples, demonstrating the variation in the crystalline structure of the samples. Hence, organic modifier (EDTA) and strontium doping played a crucial role in tempering the HAp crystallinity.

Furthermore, Table 1 indicates the lattice mis-representation and cell parameters of all the synthesized HANRs samples. The pure HANRs sample shows the lattice value as $a = b = 9.3824$ *Å* and $c = 6.8450$ *Å*. But, SrHANRs-3 sample exhibits a reduced lattice value as $a = b = 9.3607$ *Å* and $c = 6.8558$ *Å*. Furthermore, the pure HANRs sample has a unit cell volume of 512.84 $Å^3$. The SrHANRs-3 sample, on the other hand, shows an increase in the unit cell volume value of about 522.47 $Å^3$. The addition of Sr leads to an increase in the unit cell volume V value in SrHANRs-3 up to 522.47 $Å^3$. It was noted that there was a decrease in lattice constants and an increase in unit cell volumes with the accumulation of Sr dopants due to the larger radius of Sr than Ca ions (Zhou *et al*. 2021). Further, it may be replacement interactions that have taken place between the Sr^{2+} and Ca^{2+} ions due to the similar ionic radius, which may lead to the lattice parameter expansion in hydroxyapatite lattice crystals (Liu *et al*. 2020). The obtained unit cell parameter outcomes indicate that the organic modifier (EDTA) and strontium doping influence the growth of HAp crystals *via* interchanging the ripening parameters. These results show that strontium ions are well incorporated into the lattice without any distortion in the structure of HAp crystals.

The FT-IR peaks of the pure HANRs, SrHANRs-1, SrHANRs-2, and SrHANRs-3 samples are revealed in Table 2 and Fig. 3. In the FT-IR spectrum, distinct peaks were obtained in the pure HANRs, demonstrating a weak peak at 474 cm^{-1} for the doubly degenerated bending mode of the PO_4^{3-} group. Similarly, PO_4^{3-} group vibration appeared at 565 cm^{-1} and 601 cm^{-1} corresponding to the tetra degenerated bending mode. The presence of PO_4^{3-} group triply degenerated asymmetric stretching vibration mode at 1025-1124 cm^{-1} band. Furthermore, 962 cm^{-1} belonged to symmetric stretching. Thus, the occurrence of the PO_4^{3-} group was signified with diverse absorption bands of 474 to 1124 cm^{-1} (Kumar *et al*. 2018b). Furthermore, bands observed at 636 cm^{-1} and 3572 cm^{-1} correspond to the

Table 2 FT-IR spectral analysis of pure HANRs and SrHANRs samples

Sample code	Wavenumber (cm^{-1})			
	Phosphate (PO_4^{3-}) group	Hydroxyl (OH^-) group	Adsorbed CO_3^{2-}	Water (H_2O)
Pure HANRs	474, 565, 601, 962, 1025-1124	636, 3572	873, 1409, 1461	1631, 3300-3600
SrHANRs-1	476, 568, 605, 960, 1020-1108	628, 3570	881, 1403, 1450	1619, 3300-3600
SrHANRs-2	472, 566, 603, 962, 1022-1114	3569	867, 1411, 1457	1621, 3300-3600
SrHANRs-3	468, 568, 603, 960, 1024-1116	3569	877, 1419, 1496	1618, 3300-3600

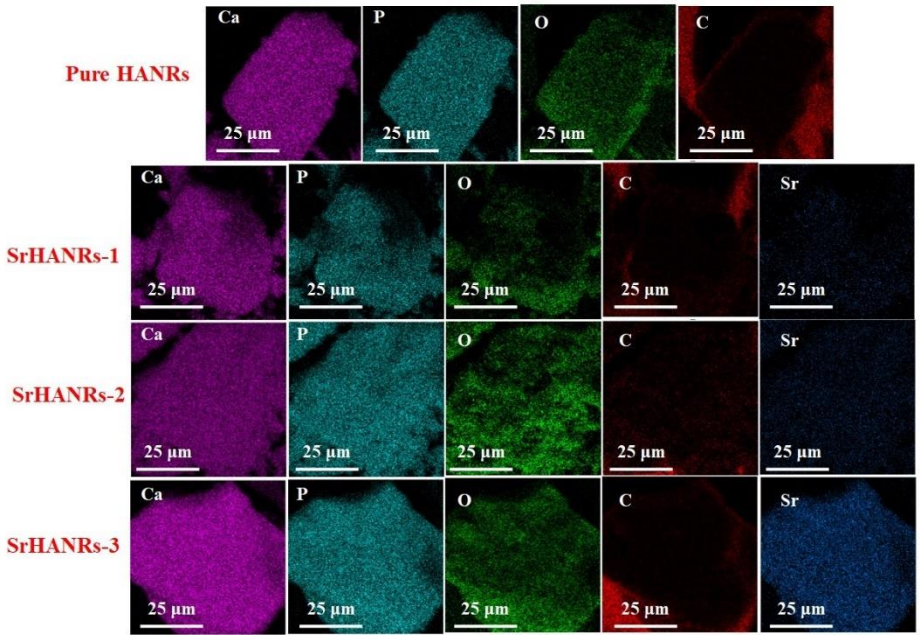

Fig. 5 Elemental mapping of pure HANRs and Sr-doped HANRs samples

presence of the OH^- group within the stretching vibration mode (Agalya *et al*. 2021b). Moreover, bands at 873, 1409, and 1461 cm^{-1} confirm the existence of CO_3^{2-}ions (Agalya *et al*. 2021a). Additional stretching vibration peaks relying on 1631 cm^{-1}, and 3300 to 3600 cm^{-1} agree with the occurrence of H_2O molecules.

The IR spectra consist of several absorption peaks of SrHANRs-1, SrHANRs-2, and SrHANRs-3 at bands ranging between 468-476, 566-568, 628, 867-881, 960-962, 1020-1116, 1403-1411, 1450-1496,1618-1621, and 3300-3600 cm^{-1} (Kumar *et al*. 2018b). The peaks at 468-476 cm^{-1} correspond to a doubly degenerative mode, while 566-568 cm^{-1} and 628 cm^{-1} rely upon the tetra degenerated bending mode of the PO_4^{3-} group. Additional peaks at 1020-1116 cm^{-1} belong to a triply degenerated mode, whereas 960-962 cm^{-1} corresponds to the symmetric stretching mode of PO_4^{3-} group. All the aforementioned absorption bands describe the presence of phosphate (PO_4^{3-}) groups in all the synthesized HAp samples (Agalya *et al*. 2021b). Furthermore, bands at 867-881, 1403-1411, and 1450-1497 cm^{-1} confirm the existence of CO_3^{2-}ions (Agalya *et al*. 2021a). Besides, the confirmation of the H_2O molecule was determined from the peaks visualized between 1618-1621, and 3300-3600 cm^{-1} corresponding to stretching vibration and bending vibration (Agalya *et al*. 2021a). Correspondingly, the present study connects with the results obtained by (Agalya *et al*. 2021a), and depicts the presence of water molecules, -OH group, and PO_4^{3-} group attributed to vibrational and stretching modes in Sr-doped materials, respectively.

Raman spectra for pure HANRs, SrHANRs-1, SrHANRs-2, and SrHANRs-3 samples, are shown in Fig. 4. The presence of the PO_4^{3-} group is indicated by the stretching vibration (ν_1) at 959-960 cm^{-1} and the triply degenerate mode (ν_3) at 1043-1044 cm^{-1} in the pure HANRs sample (De Oliveira *et al*. 2001). Moreover, weak peaks were perceived at 430-432 cm^{-1} assigned to double degenerate mode (ν_2) whereas 586-588 cm^{-1} denoted tetra degenerate bending mode (ν_4) for pure HANRs and other synthesized samples (SrHANRs-1, SrHANRs-2, and SrHANRs-3). The increase in the concentration of dopants that densifies broader peaks due to the incorporation of Sr-ions into the lattice was observed for SrHANRs-3 (Cheng *et al*. 2019).

The pure HANRs sample EDX results revealed the presence of phosphorus (P), carbon (C), calcium (Ca), and oxygen (O), which are well dispersed depending on the percentage of specific elements in Fig. 5. In addition to that, Sr-doped samples (SrHANRs-1, SrHANRs-2, and SrHANRs-3) indicate the distribution of strontium depending on its concentration during synthesis. However, a much lesser distribution could be witnessed with SrHANRs-1, whereas, a higher contribution of strontium was reported with

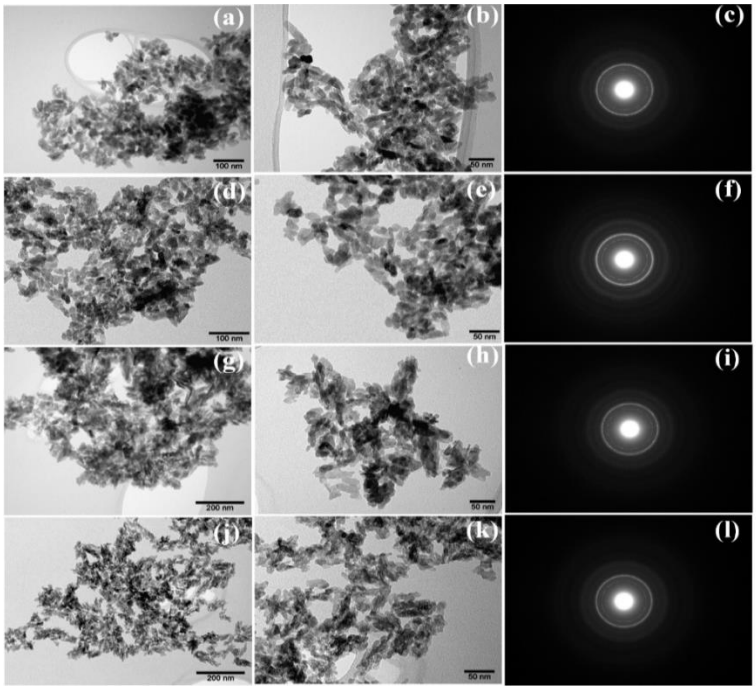

Fig. 6 TEM images and corresponding SAED pattern (a,b,c) pure HANRs, (d,e,f) SrHANRs-1, (g,h,i) SrHANRs-2, (j,k,l) SrHANRs-3

Table 3 Quantitative elemental composition of pure HANRs and SrHANRs samples

Sample code	Elements (wt.%)				
	Ca	P	O	C	Sr
Pure HANRs	32.6	17.6	43.1	6.7	--
SrHANRs-1	31.9	16.6	43.4	7.3	0.9
SrHANRs-2	29.9	16.5	42.2	7.6	1.8
SrHANRs-3	25.1	14.3	45.2	7.4	8.0

SrHANRs-3. Table 3 reports on the presence of elemental composition in the synthesized pure HANRs, SrHANRs-1, SrHANRs-2, and SrHANRs-3 samples. The obtained result reveals that the elemental configuration was found to be dissimilar among the produced samples. The ratio of the Ca/P in samples was found to be in the order of 1.85, 1.92, 1.81, and 1.75 for the samples pure HANRs, SrHANRs-1, SrHANRs-2, and SrHANRs-3, respectively. Further, it specifies that the attained outputs originate as non-stoichiometric HANRs. In addition, the strontium presence in the obtained samples was confirmed and recorded to be 0.9, 1.8, 8.0 concerning Sr/(Ca+Sr) %. Hence, the theoretical ratio and investigational ratio are almost the same, and the incorporation of Sr^{2+} in the crystal lattice of HANRs is evident.

The pure HANRs, SrHANRs-1, SrHANRs-2, and SrHANRs-3 samples were subjected to TEM analysis to reveal their morphological nature, and the perceived results are represented in Fig. 6. The pure HANRs were estimated to be 5-10 nm in width and 20-40 nm in length as elongated mesoporous nanorods, with less agglomeration (Fig. 6(a) and 6(b)). This result varies with the size of the obtained SrHANRs-1 nanoparticles, which have a width of 6-12 nm and a length of 25-45 nm (Fig. 6(d) and 6(e)). Meanwhile, SrHANRs-2 particles are mesoporous nanorods with a width of 8–15 nm and a length of 30-50 nm (Fig. 6(g) and 6(h)). Additionally, SrHANRs-3 samples have mesoporous nanorods with width of 10-30 nm and length of 40-60 nm (Fig. 6(j) and 6(k)). Hence, the synthesis of HANRs with diverse porosity, morphology, and sizes can be generated using the EDTA-enabled microwave-assisted method. In the case study described by Carvalho *et al.* (2020) the TEM micrographs visualized the development of similar SrHAp nanomaterials.

SAED patterns in Fig. 6 (c), (f), (i) and (l) shows the crystallinity of the pure HANRs, SrHANRs-1, SrHANRs-2, and SrHANRs-3 samples. The SAED patterns are well matched with the XRD patterns, which confirms that the acquired powders are pure crystalline.

HAp nanoparticles are primarily constructed through the synthesis of calcium phosphate. The constant maintenance of several parameters such as pH, temperature, and pressure results in the strong ionic interaction between the calcium and phosphate, ultimately creating an elongated crystalline structure along the *c*-axis, which in turn leads to the formation of rod-like structures from amorphous structures. EDTA played a major role in the formation of long nanorod-like structures called HANRs. Nanorods (NRs) are formed by EDTA binding the nuclei of HAp together so their faces with diverse surface energies can hold one another in their hands (Ju *et al.* 2016, Wang *et al.* 2012). This energy variance led to the formation of elongated chain-like crystal structure of particles. As a result, long nanorod-like configurations are obtained after the ripening process (Ju *et al.* 2016). As was also observed, the prominence of EDTA is used as an excellent chelating agent, which helps in the synthesis of nanoparticles (Deng *et al.* 2019).

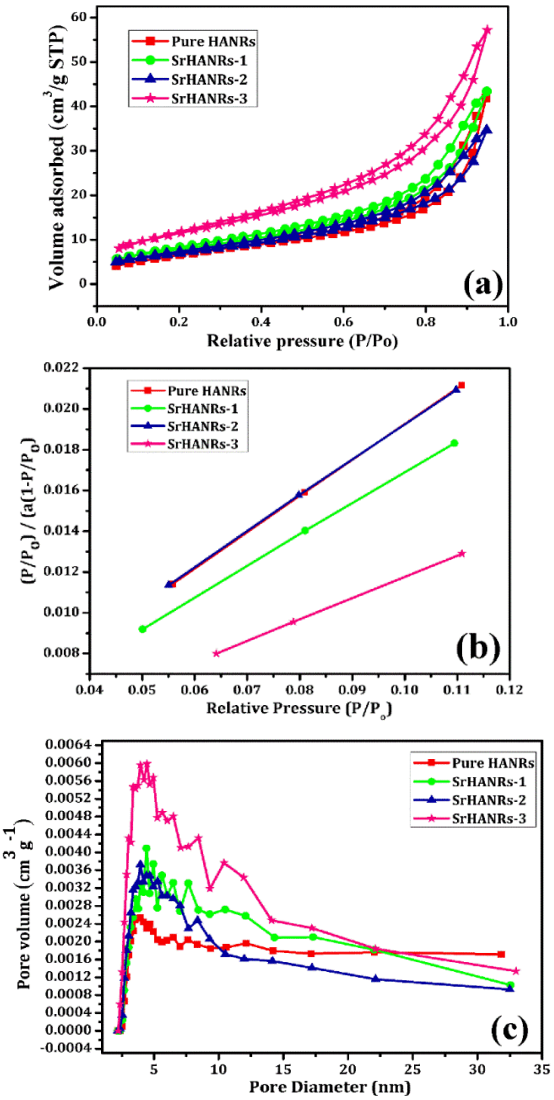

Fig. 7 (a) Nitrogen adsorption-desorption isotherms, (b) BET line, and (c) BJH-KJS pore-size distributions of pure HANRs and Sr-doped HANRs samples

Indeed, the investigation of pure HANRs, SrHANRs-1, SrHANRs-2, and SrHANRs-3 for their porous structures included the following: nitrogen adsorption/desorption isotherm in Fig. 7(a). An indication of the pore structure was usually an isotherm that demonstrated a waveform that showed an H1 hysteresis loop by type IV curve (Yan *et al*., 2001). Thus, results indicate the mesoporous structural confirmation in all the synthesized Sr doped and pure HANRs samples displays an H3 type hysteresis loop (Fig. 7(a)). Brunauer−Emmett−Teller (BET) analysis figures out a BET straight line indicating the surface area of all the samples, including pure HANRs and Sr doped HANRs in Fig. 7(b), signifying perfection in the measurement of the surface area. Pure HANRs, SrHANRs-1, SrHANRs-2, and SrHANRs-3 denote the surface areas of 75, 84, 102, and 134 $m^2\ g^{-1}$, respectively. As a result, fundamental properties such as morphology, size, surface area, composition, dimension, and polydispersity typically govern the performance of HAp nanoparticle formation (Miyajima *et al*. 2021). In addition to these parameters, surface area deviation may be caused by the incorporation of Sr, which causes a change in their morphology. Consequently, the addition of EDTA helps in changing the morphology and surface area of the HANRs. To give some idea of the benefits of our approach, it is important to calculate the pore volume and diameter of the synthesized samples using BJH-KJS methods. Correspondingly, pore volume contributes to 0.0436, 0.0499, 0.0625, and 0.0816 cm^3g^{-1} for pure HANRs, SrHANRs-1, SrHANRs-2, and SrHANRs-3 samples, whereas 3.93, 4.00, 4.46, and 4.47 nm literally denote pore diameter (at PSD peak maximum), respectively (Fig. 7(c)).

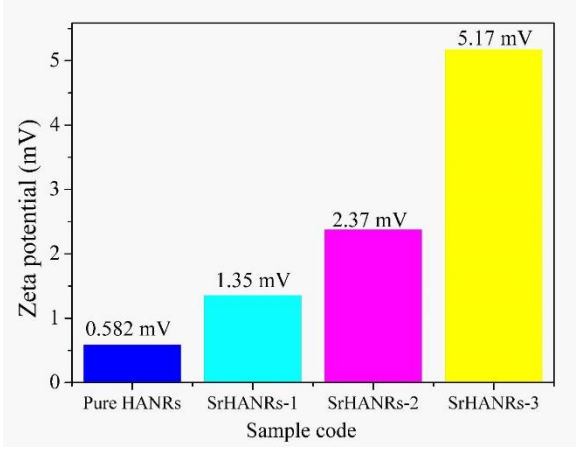

Fig. 8 Zeta potential of the synthesized pure HANRs and Sr doped HANRs nanoparticles

This section outlines the significance of the soft template method for the fabrication of HAp nanoparticles. This investigation also brings forward the perception of using EDTA as a soft template, which leads to the formation of chelating rings by packing itself around the calcium ions with four atoms of oxygen and two atoms of nitrogen, and when the above chelating rings are removed by microwave-assisted hydrothermal treatment, leads to the fabrication of various types of mesoporous structures exhibiting different pore sizes and pore volumes in pure HANRs and Sr-doped HANRs. Mesoporosity is one of the characteristics of morphology involving making contact with the living tissues, which facilitates wide applications in protein or drug delivery transporters. On the other hand, using templates (Ko *et al*. 2021), intermediated methods, and microwave-assisted methods (Butt *et al*. 2020, Głowniak *et al*. 2021) is also encouraged for the synthesis of mesoporous structures. Therefore, a new approach of using a combined EDTA-enabled microwave-assisted hydrothermal strategy is employed for the synthesis of HANRs. This novel material has the morphological structures, dimensions, and surface area of HANRs synthesized for bone fillers and regeneration applications.

The results showed the presence of zeta potential in both the doped and undoped HANRs samples, as denoted in Fig. 8. The pure HANRs, SrHANRs-1, SrHANRs-2, and SrHANRs-3 had zeta potential values of 0.582 mV, 1.35 mV, 2.37 mV, and 5.17 mV, respectively. The doping of Sr

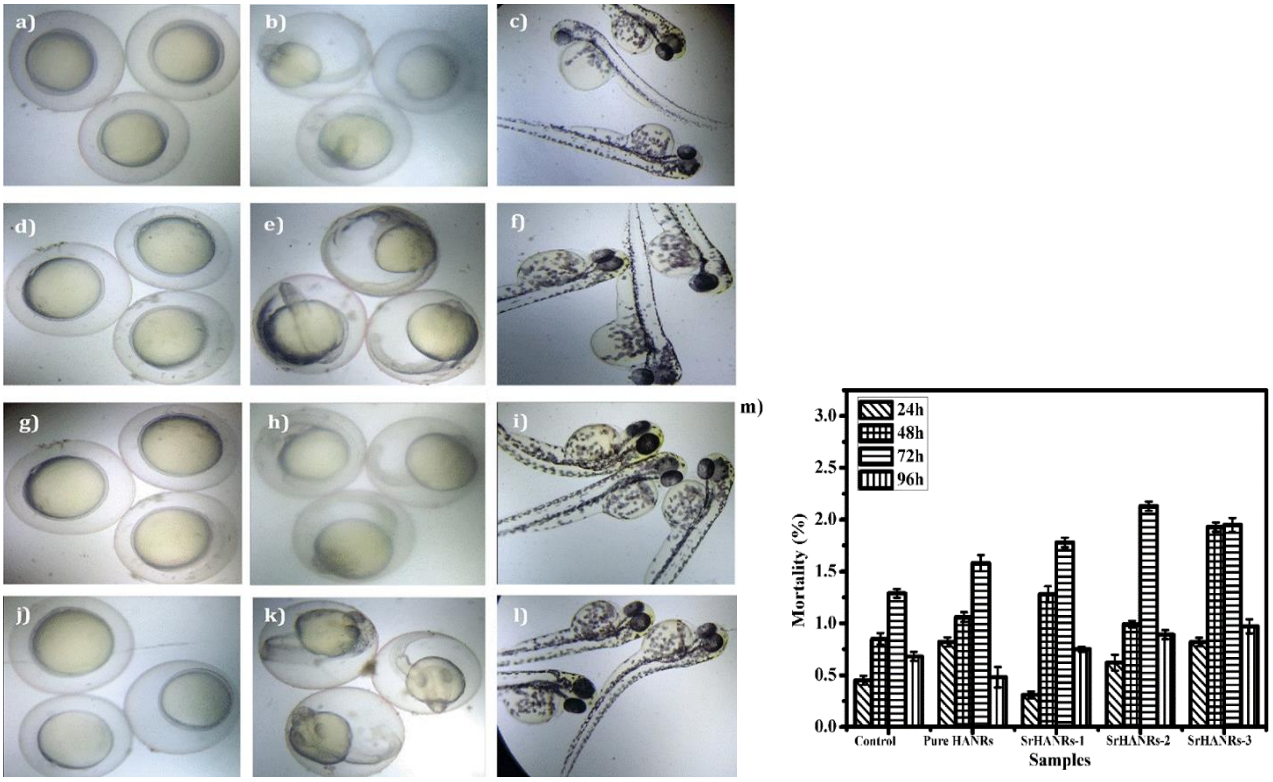

Fig. 9 Images representing the Zebrafish embryos with hours post fertilization (hpf). Control after 24 hpf (a), 48 hpf (b), and 96 hpf (c), Pure HANRs (250 µg/ml) treated after 24 hpf (d), 48 hpf (e), and 96 hpf (f), SrHANRs-1 (250 µg/ml) treated after 24 hpf (g), 48 hpf (h), and 96 hpf (i), SrHANRs-3 (250 µg/ml) treated after 24 hpf (j), 48 hpf (k), and 96 hpf (l), Bar graph (m) represents the mortality (death rate) % of prepared HANRs with respect to time and concentration

ions shifts charges from lower positive values to higher positive values. The increase in zeta potential values denotes the substitution of strontium ions. Thus, it is evident that the assimilation of Sr ions distresses the surface charges of the hydroxyapatite materials, affecting the zeta potential values (Fuseini *et al*. 2020). As a result, the charge was shifted to the higher positive with the final doping of Sr ions. It is also reported that Sr doping in bioactive glass also increased the zeta potential on the higher positive side (Amudha *et al*. 2020).

A key strength of research is that positive zeta potential and high BET surface area with better pore size distribution are factors responsible for cell proliferation. However, the designed HANRs must be ultimately suitable for attachment to living cells and tissues in vertebrates for bone regeneration. So, it is necessary to understand the requirements of HAp that allow researchers to improve the material in a way that will be similar to normal bone. Thus, biocompatibility tests are to be evaluated to check whether the synthesized biomaterial is suitable for bony replacements.

Further testing of the biocompatibility and toxicity evaluation was performed using zebrafish (*Danio rerio*), a model closely related to the human genome. The *in vivo* toxicity study of pure HANRs, SrHANRs-1, SrHANRs-2, and SrHANRs-3 samples treated with an hour post-fertilization (hpf) is depicted in Fig. 9. Initially, the embryos were screened to visualize its primary stage under the microscope. Later, doped and undoped HANRs were diluted with various concentrations (25-250 µg/ml) and added to Hank's solution. The toxic effects were screened after hpf at 24 to 96 h, respectively. Fig. 9 (a-c) represents the control samples (without the addition of HANRs) after 24, 48, and 96 hpf while, Fig. 9 (d-f) corresponds to the pure HANRs (250 µg/ml) with the same hpf. Meanwhile, Fig. 9 (g-i) denotes SrHANRs-1 (250 µg/ml) and Fig. 9 (j-l) represents SrHANRs-3 (250 µg/ml) at the aforementioned hpf. The mortality or death rate of zebrafish was not observed at higher concentrations of NRs, with significant additions at 24, 48, and 96 hpf (Fig. 9(m)). Also, there was no delay in the hatching time. Further, no significant changes on the development of the tail, head and eyes were also observed. Hence, this study reveals the non-toxic nature of the materials, which is highly recommended for use in bone replacements.

The results of non-toxicity are similar to Sengam *et al*. (2022), in their studies, they synthesized gold and silver nanoparticles using N-myristoyltaurine and evaluated the toxicity in zebrafish model (Megarajan *et al*. 2022). They confirmed that both the gold and silver nanoparticles are non-toxic in nature. In another study by Subeena *et al*. (2022), the CuO nanoparticles were synthesized using *Salacia reticulate* leaf extract, and it also showed lower toxicity towards the zebrafish compared to the chemically synthesized CuO nanoparticles (Subeena *et al*. 2022).

Furthermore, in another study by Madhubala *et al*. (2019), also showed that α-Fe_2O_3 nanoparticles synthesized

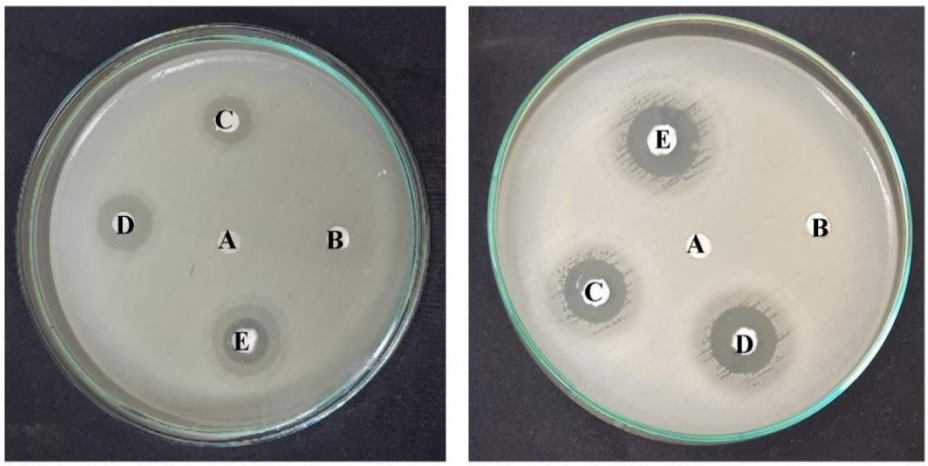

Fig. 10 Antibacterial activity of A) commercial HANRs, B) pure HANRs, C) SrHANRs-1, D) SrHANRs-2, E) SrHANRs-3

Table 4 Antibacterial activity of pure HANRs and Sr doped HANRs

Microorganisms	Zone of inhibition [Mean ± SD (mm)]			
	Pure HANRs (100 µg/ml)	SrHANRs-1 (100 µg/ml)	SrHANRs-2 (100 µg/ml)	SrHANRs-3 (100 µg/ml)
Staphylococcus aureus (MTCC 7443)	-	09.32±0.43	11.30±0.14	14.32±0.21
Klebsiella pneumoniae (MTCC 7407)	-	16.04±0.32	18.26±0.42	19.34±0.16

by hydrothermal method showed non-toxic nature towards the zebrafish (Madhubala *et al*. 2019). They also confirmed that the hatching rate was not affected due to the α-Fe_2O_3 nanoparticles exposure. However, a study by Srinivasan *et al*. (2019) showed that green synthesized TiO_2 using *Sesbania grandiflora* showed significant toxicity in zebrafish embryos (Srinivasan *et al*. 2019). They observed that the TiO_2 nanoparticles delayed the hatching rate in the zebrafish embryos.

Fig. 10 and Table 4 disclose the antibacterial competence of pure HANRs, SrHANRs-1, SrHANRs-2, and SrHANRs-3 against *K. pneumoniae* (gram-negative) and *S. aureus* (gram-positive). The formation of a zone of inhibition is recognized as 09.32 ± 0.43 mm (for SrHANRs-1) and 14.32 ± 0.21 mm (for SrHANRs-3) against *S. aureus*. Moreover, an inhibitory zone with 16.04 ± 0.32 mm (for SrHANRs-1) and 19.34 ± 0.16 mm (for SrHANRs-3) against *K. pneumoniae* was also observed. As a result, SrHANRs-3 has the highest inhibitory zones against organisms compared to the other synthesized nanorods. Hence, penetration of SrHANRs-3 effectively affects the cellular activity of the intracellular enzymes and other biomolecules, which leads to dysfunction of cellular activities, leading to cell death (Punjabi *et al*. 2018, Supraja *et al*. 2017, Vizhi *et al*. 2016). Since pure HAp particles lack antibacterial activity, they have no intrinsic features to deaminize bacterial effects causing implant-related infections. Thus, current implant- ology requires a shift to the use of Sr-doped HAp nano-particles to avoid implant failures due to pathogen intervention.

These results have led to high levels of agreement with similar findings reported by Nafiseh *et al*. (2021), who tested Sr-doped bioactive glasses as antibacterial agents (Baheiraei *et al*. 2021). They found that the biocidal activity of the bioactive glasses increased with the addition of Sr, specifically against *E. coli* and *S. aureus* (Baheiraei *et al*. 2021). Lie *et al*. (2016) also studied the biological function of Sr substituted bioactive glass, which was found to have effective biological activity and bactericidal properties (Liu *et al*. 2016). Further, correlation with the study reported by Brauer *et al*. (2013) helps to widen its application because its antibacterial action must be inherent for superlative and comprehensive implementation. Thus, based on the excellent properties of SrHANRs produced *via* the EDTA-enable microwave-mediated method using *Anodontia alba* seashells, it could be an excellent bio-apatite for resolving bacterial infections following bone implant applications.

4. Conclusions

In conclusion, the present investigation helped in the synthesis of biomaterials using strontium-doped hydroxy-apatite, which signifies its role in clinical applications. Postsurgical infections occur due to implant-related infectious agents that lead to implant failure. This major problem could be overcome using a biomaterial that is biocompatible and consists of osteogenic features. Such problems could be greatly resolved by the use of SrHANRs, synthesized *via* an EDTA-enabled microwave-assisted

method bearing a bactericidal effect and exhibiting much more effective activity because of their doping effect. EDTA-enabled synthesis helps in the fabrication of mesoporous crystalline structures in the synthesized Sr-doped samples (SrHANRs-1, SrHANRs-2, and SrHANRs-3), maintaining appropriate pore size, surface area, shape, size, and pore volume. The characteristic study result reveals that the produced nanorods are hexagonal HANRs. Additionally, it has been found that the synthesized HANRs have potential bactericidal action and are non-toxic, which helps to develop bio-apatite. The findings show that EDTA-assisted microwave hydrothermal mediated approaches using *Anodontia alba* seashells can yield Sr-doped mesoporous HANRs with tunable nanoscale properties for implant applications.

Acknowledgments

E.-B. Cho and Gopalu Karunakaran were supported by Brain Pool Program through the National Research Foundation of Korea (NRF) funded by the Ministry of Science and ICT (Grant no. 2022H1D3A2A02044281).

References

Abifarin, J.K., Obada, D.O., Dauda, E.T. and Dodoo-Arhin, D. (2019), "Experimental data on the characterization of hydroxyapatite synthesized from biowastes", *Data Br*., **26**, 104485. https://doi.org/10.1016/j.dib.2019.104485.

Agalya, P., Saravanan, T., Kumar, G.S., Cholan, S., Karunakaran, G. and Van Minh, N. (2021a), "Surfactant-assisted microwave synthesis of luminescent/magnetic bifunctional hydroxyapatite nanorods for dual-model imaging", *Optik*, **225**, 165564. https://doi.org/10.1016/j.ijleo.2020.165564.

Agalya, P., Suresh Kumar, G., Srinivasan, R., Prabu, K.M., Karunakaran, G., Cholan, S., Kolesnikov, E. and Kim, M. (2021b), "Hydroxyapatite-based antibacterial bio-nanomaterials: An insight into the synthesis using mussel shell as a calcium source, physicochemical properties, and nanoindentation characteristics", *Appl. Phys. A Mater. Sci. Proc*., **127**, 589. https://doi.org/10.1007/s00339-021-04739-8.

Ahmed, T., Baidya, S., Sharma, B.C., Malek, M., Das, K.K., Acharjee, M., Munshi, S.K. and Noor, R. (2013), "Identification of drug-resistant bacteria among export quality shrimp samples in Bangladesh", *Asian J. Microbiol. Biotechnol. Environ. Sci*., **15**, 655-660. https://doi.org/10.1093/ajcp/45.4_ts.493.

Amudha, S., Ramya, J.R., Arul, K.T., Deepika, A., Sathiamurthi, P., Mohana, B., Asokan, K., Dong, C.L. and Kalkura, S.N. (2020), "Enhanced mechanical and biocompatible properties of strontium ions doped mesoporous bioactive glass", *Compos. Part B Eng*., **196**, 108099. https://doi.org/10.1016/j.compositesb.2020.108099

Apsana, G., George, P.P., Devanna, N. and Yuvasravana, R. (2018), "Biomimetic synthesis and antibacterial properties of strontium oxide nanoparticles using ocimum sanctum leaf extract", *Asian J. Pharm. Clin. Res*., **11**, 384-389. https://doi.org/10.22159/ajpcr.2018.v11i3.20858.

Arcos, D. and Vallet-Regí, M. (2020), "Substituted hydroxyapatite coatings of bone implants", *J. Mater. Chem. B*., **8**, 1781-1800. https://doi.org/10.1039/c9tb02710f.

Ayyanar, C.B., Marimuthu, K., Gayathri, B. and Sankarrajan. (2020), "Characterization and in vitro cytotoxicity evaluation of fish scale and seashell derived nano-hydroxyapatite high-density polyethylene composite", *Polym. Polym. Compos*., **29**(9), 1534-1542. https://doi.org/10.1177/0967391120981551.

Baheiraei, N., Eyni, H., Bakhshi, B., Najafloo, R. and Rabiee, N. (2021), "Effects of strontium ions with potential antibacterial activity on in vivo bone regeneration", *Sci. Rep*., **11**, 8745. https://doi.org/10.1038/s41598-021-88058-1.

Balakrishnan, S., Padmanabhan, V.P., Kulandaivelu, R., Sankara Narayanan Nellaiappan, T.S., Sagadevan, S., Paiman, S., Mohammad, F., Al-Lohedan, H.A., Obulapuram, P.K. and Oh, W.C. (2021) "Influence of iron doping towards the physico-chemical and biological characteristics of hydroxyapatite", *Ceram. Int*., **47**, 5061-5070. https://doi.org/10.1016/j.ceramint.2020.10.084.

Balaz, M., Balazova, L., Kovačova, M., Daneu, N., Salayova, A., Bedlovicova, Z. and Tkacikova, L. (2019), "The relationship between precursor concentration and antibacterial activity of biosynthesized Ag nanoparticles", *Adv. Nano Res*., **7**(2), 125-134. https://doi.org/10.12989/anr.2019.7.2.125.

Balu, S., Sundaradoss, M.V., Anra, S. and Jeevanandam, J. (2020), "Facile biogenic fabrication of hydroxyapatite nanorods using cuttlefish bone and their bactericidal and biocompatibility study", *Beilstein J. Nanotechnol*., **11**, 285-295. https://doi.org/10.3762/bjnano.11.21.

Bhat, S., Uthappa, U.T., Altalhi, T., Jung, H.Y. and Kurkuri, M.D. (2021), "Functionalized porous hydroxyapatite scaffolds for tissue engineering applications: A focused review", *ACS Biomater. Sci. Eng*., **8**(10), 4039-4076. https://doi.org/10.1021/acsbiomaterials.1c00438.

Bhattacharjee, A., Hassan, R., Gupta, A., Verma, M., Murugan, P.A., Sengupta, P., Saravanan, M., Manna, I. and Balani, K. (2020), "Effect of Zn and Co doping on antibacterial efficacy and cytocompatibility of spark plasma sintered hydroxyapatite", *J. Am. Ceram. Soc*., **103**, 4090-4100. https://doi.org/10.1111/jace.17077.

Bolli, E., Kaciulis, S., Mezzi, A., Ambrogi, V., Nocchetti, M., Latterini, L., Di Michele, A. and Padeletti, G. (2021), "Hydroxyapatite functionalized calcium carbonate composites with ag nanoparticles: An integrated characterization study", *Nanomaterials*, **11**(9), 2263. https://doi.org/10.3390/nano11092263.

Brauer, D.S., Karpukhina, N., Kedia, G., Bhat, A., Law, R. V., Radecka, I. and Hill, R.G. (2013), "Bactericidal strontium-releasing injectable bone cements based on bioactive glasses", *J. R. Soc. Interf*., **10**, 20120647. https://doi.org/10.1098/rsif.2012.0647.

Butt, F.K., Hauenstein, P., Kosiahn, M., Garlyyev, B., Dao, M., Lang, A., Scieszka, D., Liang, Y. and Kreuzpaintner, W. (2020), "An innovative microwave-assisted method for the synthesis of mesoporous two dimensional g-C3N4: A revisited insight into a potential electrode material for supercapacitors", *Microporous Mesoporous Mater*., **294**, 109853. https://doi.org/10.1016/j.micromeso.2019.109853.

Cai, Z., Wang, X., Zhang, Z., Han, Y., Luo, J., Huang, M., Zhang, B. and Hou, Y. (2019), "Large-scale and fast synthesis of nano-hydroxyapatite powder by a microwave-hydrothermal method", *RSC Adv*., **9**, 13623-13630. https://doi.org/10.1039/c9ra00091g.

Carvalho, E.V., de Paula, D.M. andrade Neto, D.M., Costa, L.S., Dias, D.F., Feitosa, V.P. and Fechine, P.B.A. (2020), "Radiopacity and mechanical properties of dental adhesives with strontium hydroxyapatite nanofillers", *J. Mech. Behav. Biomed. Mater*., **101**, 103447. https://doi.org/10.1016/j.jmbbm.2019.103447.

Cheng, G., Zhang, Y., Yin, H., Ruan, Y., Sun, Y. and Lin, K. (2019), "Effects of strontium substitution on the structural distortion of hydroxyapatite by rietveld refinement and Raman Spectroscopy", *Ceram. Int*., **45**, 11073-11078.

https://doi.org/10.1016/j.ceramint.2019.02.194
De Oliveira, L.M., Rossi, A.M. and Lopes, R.T. (2001), "Dose response of A-type carbonated apatites prepared under different conditions", *Radiat. Phys. Chem.*, **61**(3-6), 485-487. https://doi.org/10.1016/S0969-806X(01)00309-7.
Deng, Y., Ye, C., Chen, G., Tao, B., Luo, H. and Li, N. (2019), "EDTA-assisted hydrothermal synthesis of flower-like CoSe2 nanorods as an efficient electrocatalyst for the hydrogen evolution reaction", *J. Energy Chem.*, **28**, 95-100. https://doi.org/10.1016/j.jechem.2018.01.022.
F. El-Maghraby, H. and E. Greish, Y. (2021), "Preparation, structural characterization, and biomedical applications of gypsum-based nanocomposite bone cements", *Novel Nanomater.*, Chapter 13. https://doi.org/10.5772/intechopen.94317.
Feng, P., Wang, K., Shuai, Y., Peng, S., Hu, Y. and Shuai, C. (2022), "Hydroxyapatite nanoparticles in situ grown on carbon nanotube as a reinforcement for poly (ε-caprolactone) bone scaffold", *Mater. Today Adv.*, **15**, 100272. https://doi.org/10.1016/j.mtadv.2022.100272.
Fu, J., Huang, L., Yu, Z., Zhang, Z. and Li, G. (2021), "Synthesis of hairpin DNA mediated Au-Ag bimetallic nanomushrooms for antibacterial application", *Adv. Nano Res.*, **11**, 73-81. https://doi.org/10.12989/anr.2021.11.1.073.
Fuseini, M., El-Shazly, A.H. and Elkady, M. (2020), "Effects of doping on zeta potential and ph of polyaniline colloidal suspension", *Mater. Sci. Forum*, **1008**, 114-120. https://doi.org/10.4028/www.scientific.net/MSF.1008.114.
Garg, D., Matai, I. and Sachdev, A. (2021), "Toward designing of anti-infective hydrogels for orthopedic implants: From lab to clinic", *ACS Biomater. Sci. Eng.*, **7**(6), 1933-1961. https://doi.org/10.1021/acsbiomaterials.0c01408.
George, R.S., Somasundaram, J., Balaji Ganesh, S. and Roy, A. (2020), "Synthesis of hydroxyapatite crystals from egg shells", *Int. J. Res. Pharm. Sci.* **11**, 1406-1411. https://doi.org/10.26452/ijrps.v11iSPL3.3422.
Głowniak, S., Szczęśniak, B., Choma, J. and Jaroniec, M. (2021), "Advances in microwave synthesis of nanoporous materials", *Adv. Mater.*, **33**, 2103477. https://doi.org/10.1002/adma.202103477.
Hwang, Y., Lee, J.S., An, H., Oh, H., Sung, D., Tae, G. and Choi, Il, W. (2021), "Hydroxyapatite-embedded levan composite hydrogel as an injectable dermal filler for considerable enhancement of biological efficacy", *J. Ind. Eng. Chem.*, **104**, 491-499. https://doi.org/10.1016/j.jiec.2021.08.040.
Jang, Y., Lee, N., Kim, J.H., Park, Y. Il, and Piao, Y. (2018), "Shape-controlled synthesis of au nanostructures using edta tetrasodium salt and their photothermal therapy applications", *Nanomaterials*, **8**(4), 252. https://doi.org/10.3390/nano8040252.
Javed, R., Zia, M., Naz, S., Aisida, S.O., Ain, N. and Ao, Q. (2020), "Role of capping agents in the application of nanoparticles in biomedicine and environmental remediation: Recent trends and future prospects", *J. Nanobiotechnol.* **18**, 172. https://doi.org/10.1186/s12951-020-00704-4.
Jenkins, R. and Snyder, R.L. (1996), "Introduction to X-ray powder diffractometry", *Introduction to X-ray Powder Diffractometry*. https://doi.org/10.1002/9781118520994.
Ju, P., Yu, Y., Wang, M., Zhao, Y., Zhang, D., Sun, C. and Han, X. (2016), "Synthesis of EDTA-assisted $CeVO_4$ nanorods as robust peroxidase mimics towards colorimetric detection of H_2O_2", *J. Mater. Chem. B*, **4**, 6316-6325. https://doi.org/10.1039/c6tb01881e.
Ko, S.W., Lee, J.Y., Rezk, A.I., Park, C.H. and Kim, C.S. (2021), "In-situ cellulose-framework templates mediated monodispersed silver nanoparticles via facile UV-light photocatalytic activity for anti-microbial functionalization", *Carbohydr. Polym.*, **269**, 118255. https://doi.org/10.1016/j.carbpol.2021.118255.
Koutu, V., Rajawat, S., Shastri, L. and Malik, M.M. (2019), "Apoptosis and inhibition of human epithelial cancer cells by ZnO nanoparticles synthesized using plant extract", *Adv. Nano Res.*, **7**, 231-239. https://doi.org/10.12989/anr.2019.7.4.231.
Kumar, G.S., Karunakaran, G., Girija, E.K., Kolesnikov, E., Minh, N. Van, Gorshenkov, M. V. and Kuznetsov, D. (2018a), "Size and morphology-controlled synthesis of mesoporous hydroxyapatite nanocrystals by microwave-assisted hydrothermal method", *Ceram. Int.*, **44**, 11257-11264. https://doi.org/10.1016/j.ceramint.2018.03.170.
Kumar, G.S., Muthu, D., Karunakaran, G., Karthi, S., Girija, E.K. and Kuznetsov, D. (2018b), "Curcuma longa tuber extract mediated synthesis of hydroxyapatite nanorods using biowaste as a calcium source for the treatment of bone infections", *J. Sol-Gel Sci. Technol.*, **86**, 610-616. https://doi.org/10.1007/s10971-018-4670-6.
Liu, J., Rawlinson, S.C.F., Hill, R.G. and Fortune, F. (2016), "Strontium-substituted bioactive glasses in vitro osteogenic and antibacterial effects", *Dent. Mater.*, **32**, 412-422. https://doi.org/10.1016/j.dental.2015.12.013.
Liu, M., Shu, M., Yan, J., Liu, X., Wang, R., Hou, Z. and Lin, J. (2021), "Luminescent net-like inorganic scaffolds with europium-doped hydroxyapatite for enhanced bone reconstruction", *Nanoscale*, **13**, 1181-1194. https://doi.org/10.1039/d0nr05608a.
Liu, Q., Xue, Z. and Xu, D. (2020), "Molecular dynamics characterization of Sr-doped biomimetic hydroxyapatite nanoparticles", *J. Phys. Chem. C*, **124**, 19704-19715. https://doi.org/10.1021/acs.jpcc.0c06391.
Madhubala, V., Kalaivani, T., Kirubha, A., Prakash, J.S., Manigandan, V. and Dara, H.K. (2019), "Study of structural and magnetic properties of hydro/solvothermally synthesized α-Fe_2O_3 nanoparticles and its toxicity assessment in zebrafish embryos", *Appl. Surf. Sci.*, **494**, 391-400. https://doi.org/10.1016/j.apsusc.2019.07.090.
Madubuonu, N., Aisida, S.O., Ahmad, I., Botha, S., Zhao, T. kai, Maaza, M. and Ezema, F.I. (2020), "Bio-inspired iron oxide nanoparticles using Psidium guajava aqueous extract for antibacterial activity", *Appl. Phys. A Mater. Sci. Proc.*, **126**, 72. https://doi.org/10.1007/s00339-019-3249-6.
Maleki-Ghaleh, H., Hossein Siadati, M., Fallah, A., Zarrabi, A., Afghah, F., Koc, B., Dalir Abdolahinia, E., Omidi, Y., Barar, J., Akbari-Fakhrabadi, A., Beygi-Khosrowshahi, Y. and Adibkia, K. (2021), "Effect of zinc-doped hydroxyapatite/graphene nanocomposite on the physicochemical properties and osteogenesis differentiation of 3D-printed polycaprolactone scaffolds for bone tissue engineering", *Chem. Eng. J.*, **426**, 131321. https://doi.org/10.1016/j.cej.2021.131321.
Megarajan, S., Ameen, F., Singaravelu, D., Islam, M.A. and Veerappan, A. (2022), "Synthesis of N-myristoyltaurine stabilized gold and silver nanoparticles: Assessment of their catalytic activity, antimicrobial effectiveness and toxicity in zebrafish", *Environ. Res.* **212**, 113159. https://doi.org/10.1016/j.envres.2022.113159.
Miyajima, H., Touji, H. and Iijima, K. (2021), "Hydroxyapatite particles from simulated body fluids with different ph and their effects on mesenchymal stem cells", *Nanomaterials*, **11**(10), 2517. https://doi.org/10.3390/nano11102517.
Molino, G., Palmieri, M.C., Montalbano, G., Fiorilli, S. and Vitale-Brovarone, C. (2020), "Biomimetic and mesoporous nano-hydroxyapatite for bone tissue application: A short review", *Biomed. Mater.*, **15**, 022001. https://doi.org/10.1088/1748-605X/ab5f1a.
Mondal, S., Dey, A. and Pal, U. (2016), "Low temperature wet-chemical synthesis of spherical hydroxyapatite nanoparticles and their in situ cytotoxicity study", *Adv. nano Res.*, **4**(4), 295-307. https://doi.org/10.12989/anr.2016.4.4.295.
Moore, H. and López, N. (1970), "A Contribution to the Ecology

of the Lamellibranch Tellina Alternata", *Bull. Mar. Sci*., **20**, 971-979.

Nakayama, M., Kajiyama, S., Kumamoto, A., Nishimura, T., Ikuhara, Y., Yamato, M. and Kato, T. (2018), "Stimuli-responsive hydroxyapatite liquid crystal with macroscopically controllable ordering and magneto-optical functions", *Nat. Commun*., **9**, 568. https://doi.org/10.1038/s41467-018-02932-7.

Naseri, H., Ghatee, M., Yazdani, A., Mohammadi, M. and Manafi, S. (2021), "Characterization of the 3YSZ/CNT/HAP coating on the Ti6Al4V alloy by electrophoretic deposition", *J. Biomed. Mater. Res. Part B Appl*., **109**, 1395-1406. https://doi.org/10.1002/jbm.b.34799.

Niehoff, N.M., Keil, A.P., O'Brien, K.M., Jackson, B.P., Karagas, M.R., Weinberg, C.R. and White, A.J. (2020), "Metals and trace elements in relation to body mass index in a prospective study of US women", *Environ. Res*., **184**, 109396. https://doi.org/10.1016/j.envres.2020.109396.

Nordin, J.A., Prajitno, D.H., Saidin, S., Nur, H. and Hermawan, H. (2015), "Structure-property relationships of iron-hydroxyapatite ceramic matrix nanocomposite fabricated using mechanosynthesis method", *Mater. Sci. Eng. C*, **51**, 294-299. https://doi.org/10.1016/j.msec.2015.03.019.

Oner, F.K., Alakent, B. and Soyer-Uzun, S. (2021), "Effect of silane A-174 modifications in the structure, chemistry, and compressive strength of PLA-HAP and PLA-β-TCP biocomposites: Toward the design of polymer-ceramic implants with high performance", *ACS Appl. Polym. Mater*., **3**, 2432-2446. https://doi.org/10.1021/acsapm.1c00054.

Paduraru, A.V., Oprea, O., Musuc, A.M., Vasile, B.S., Iordache, F. and Andronescu, E. (2021), "Influence of terbium ions and their concentration on the photoluminescence properties of hydroxyapatite for biomedical applications", *Nanomaterials*, **11**(9), 2442. https://doi.org/10.3390/nano11092442.

Pilmane, M., Salma-Ancane, K., Loca, D., Locs, J. and Berzina-Cimdina, L. (2017), "Strontium and strontium ranelate: Historical review of some of their functions", *Mater. Sci. Eng. C* **78**, 1222-1230. https://doi.org/10.1016/j.msec.2017.05.042.

Pors Nielsen, S. (2004), "The biological role of strontium", *Bone*, https://doi.org/10.1016/j.bone.2004.04.026.

Punjabi, K., Mehta, S., Yedurkar, S., Jain, R., Mukherjee, S., Kale, A. and Deshpande, S. (2018), "Extracellular synthesis of silver nanoparticle by *Pseudomonas* hibiscicola-Mechanistic approach", *Adv. Nano Res*., **6**(1), 81-92. https://doi.org/10.12989/anr.2018.6.1.081.

Rabiei, M., Palevicius, A., Monshi, A., Nasiri, S., Vilkauskas, A. and Janusas, G. (2020), "Comparing methods for calculating nano crystal size of natural hydroxyapatite using X-ray diffraction", *Nanomaterials*, **10**, 1-21. https://doi.org/10.3390/nano10091627.

Ranjeh, M., Masjedi-Arani, M., Salavati-Niasari, M. and Moayedi, H. (2020), "EDTA-modified sol-gel synthesis of monoclinic Li_2MnO_3 nanoparticles as an effective photocatalyst for degradation of organic dyes", *J. Mol. Liq*., **300**, 112292. https://doi.org/10.1016/j.molliq.2019.112292.

Sabeena, G.S.R.E.P., Alhadlaq, H.A., Mohan, R.G.A. and Ahamed, M. (2022), "Green and chemical synthesis of CuO nanoparticles: A comparative study for several in vitro bioactivities and in vivo toxicity in zebrafish embryos", *J. King Saud Univ. Sci*., **34**, 102092. https://doi.org/10.1016/j.jksus.2022.102092.

Shuai, C., Peng, B., Feng, P., Yu, L., Lai, R. and Min, A. (2022), "In situ synthesis of hydroxyapatite nanorods on graphene oxide nanosheets and their reinforcement in biopolymer scaffold", *J. Adv. Res*., **35**, 13-24. https://doi.org/10.1016/j.jare.2021.03.009.

Shuai, C., Yang, W., Feng, P., Peng, S. and Pan, H. (2021), "Accelerated degradation of HAP/PLLA bone scaffold by PGA blending facilitates bioactivity and osteoconductivity", *Bioact. Mater*., **6**, 490-502. https://doi.org/10.1016/j.bioactmat.2020.09.001.

Siswanto, Hikmawati, D. and Aminatun, Supardi, A. (2020), "Molarity optimization of calcium hydroxide in the forming of bioceramic hydroxyapatite from nano coral by precipitation method", *Moroccan J. Chem*., **8**, 24-31. https://doi.org/10.48317/IMIST.PRSM/morjchem-v8i1.19121.

Srinivasan, M., Venkatesan, M., Arumugam, V., Natesan, G., Saravanan, N., Murugesan, S., Ramachandran, S., Ayyasamy, R. and Pugazhendhi, A. (2019), "Green synthesis and characterization of titanium dioxide nanoparticles (TiO_2 NPs) using Sesbania grandiflora and evaluation of toxicity in zebrafish embryos", *Proc. Biochem*., **80**, 197-202. https://doi.org/10.1016/j.procbio.2019.02.010.

Suchánková, P., Kukleva, E., Nykl, E., Nykl, P., Sakmár, M., Vlk, M. and Kozempel, J. (2020), "Hydroxyapatite and titanium dioxide nanoparticles: Radiolabelling and in vitro stability of prospective theranostic nanocarriers for 223ra and 99mtc", *Nanomaterials*, **10**, 1-12. https://doi.org/10.3390/nano10091632.

Sudha, K.G., Ali, S., Karunakaran, G., Kowsalya, M., Kolesnikov, E. and Rajeshkumar, M.P. (2020), "Eco-friendly synthesis of ZnO nanorods using Cycas pschannae plant extract with excellent photocatalytic, antioxidant, and anticancer nanomedicine for lung cancer treatment", *Appl. Organomet. Chem*. **34**, e5511. https://doi.org/10.1002/aoc.5511.

Sun, W., Fan, J., Wang, S., Kang, Y., Du, J. and Peng, X. (2018), "Biodegradable drug-loaded hydroxyapatite nanotherapeutic agent for targeted drug release in tumors", *ACS Appl. Mater. Interfaces* **10**, 7832-7840. https://doi.org/10.1021/acsami.7b19281.

Supraja, N., Avinash, B. and Prasad, T.N.V.K.V. (2017), "Nelumbo nucifera extracts mediated synthesis of silver nanoparticles for the potential applications in medicine and environmental remediation", *Adv. Nano Res*., **5**(4), 373-392. https://doi.org/10.12989/anr.2017.5.4.373.

Supraja, N., Dhivya, J., Prasad, T.N.V.K.V. and David, E. (2018), "Synthesis, characterization and dose dependent antimicrobial and anticancerous efficacy of phycogenic (Sargassum muticum) silver nanoparticles against Breast Cancer Cells (MCF 7) cell line", *Adv. Nano Res*., **6**(2), 183-200. https://doi.org/10.12989/anr.2018.6.2.183.

Szabó, A.S. (2017), "Investigation of the strontium content of foods and the biological role of strontium", *Elelmiszervizsgalati Kozlemenyek*, **63**, 1774-1789.

Tao, B., Lin, C., Guo, A., Yu, Y., Qin, X., Li, K., Tian, H., Yi, W., Lei, D. and Chen, L. (2021), "Fabrication of copper ions-substituted hydroxyapatite/polydopamine nanocomposites with high antibacterial and angiogenesis effects for promoting infected wound healing", *J. Ind. Eng. Chem*., **104**, 345-355. https://doi.org/10.1016/j.jiec.2021.08.035.

Um, S.H., Chung, Y.W., Seo, Y., Seo, H., Ok, M.R., Kim, Y.C., Han, H.S., Chung, J.J., Edwards, J.R. and Jeon, H. (2020), "Robust hydroxyapatite coating by laser-induced hydrothermal synthesis", *Adv. Funct. Mater*., **30**, 2005233. https://doi.org/10.1002/adfm.202005233.

Vizhi, D.K., Supraja, N., Devipriya, A., Tollamadugu, N.V.K.V.P. and Babujanarthanam, R. (2016), "Evaluation of antibacterial activity and cytotoxic effects of green AgNPs against Breast Cancer Cells (MCF 7)", *Adv. Nano Res*., **4**, 129-143. https://doi.org/10.12989/anr.2016.4.2.129.

Wang, L., Sun, Y., Li, C., Wang, Yaozu, Ma, X., Wang, Yandi, Li, S., Zhang, Z., Ma, P. and Cui, G. (2012), "Morphology-controlled CaMoO4 nanorods via a facile microwave-assisted EDTA chelating agent process", *Cryst. Res. Technol*., **47**, 1231-1236. https://doi.org/10.1002/crat.201200148.

Wei, W. and Dai, H. (2021), "Articular cartilage and osteochondral tissue engineering techniques: Recent advances and

challenges", *Bioact. Mater.* **6**, 4830-4855. https://doi.org/10.1016/j.bioactmat.2021.05.011.

Wood, E.J. (2004), "Biochemistry: The chemical reactions of living cells", *Biochem. Mol. Biol. Educ.*, **32**, 62-63. https://doi.org/10.1002/bmb.2004.494032010298.

Yan, L., Li, Y., Deng, Z.X., Zhuang, J. and Sun, X. (2001), "Surfactant-assisted hydrothermal synthesis of hydroxyapatite nanorods", *Int. J. Inorg. Mater.*, **3**, 633-637. https://doi.org/10.1016/S1466-6049(01)00164-7.

Yi, Y., Zhang, Y., Wang, Y., Shen, L., Jia, M., Huang, Y., Hou, Z. and Zhuang, G. (2014), "Ethylenediaminetetraacetic acid as capping ligands for highly water-dispersible iron oxide particles", *Nanosc. Res. Lett.*, **9**, 27. https://doi.org/10.1186/1556-276X-9-27.

Yuan, Q., Zhang, Z., Yang, Y., Jian, Y., Li, R., Dai, X., Wu, W., Zhong, J. and Chen, C. (2021), "Synthesis, characterization and biological performance study of Sr-doped hydroxyapatite/ chitosan composite coatings", *Mater. Chem. Phys.*, **270**, 124752. https://doi.org/10.1016/j.matchemphys.2021.124752.

Zhou, Y., Li, W., Jiang, X., Sun, Y., Yang, H., Liu, Q., Cao, Y., Zhang, Y. and Cheng, H. (2021), "Synthesis of strontium (Sr) doped hydroxyapatite (HAp) nanorods for enhanced adsorption of Cr (VI) ions from wastewater", *Ceram. Int.*, **47**, 16730-16736. https://doi.org/10.1016/j.ceramint.2021.02.243.

CC